AFRL-VS-HA-TR-2004-1037

IMAGING AND FORECASTING OF IONOSPHERIC STRUCTURES AND THEIR SYSTEM IMPACTS

Bodo Reinisch
Gary Sales

University of Massachusetts Lowell
Center for Atmospheric Research
600 Suffolk Street
Lowell, MA 01854

5 December 2004

Scientific Report No. 1

AIR FORCE RESEARCH LABORATORY
Space Vehicles Directorate
29 Randolph Rd
AIR FORCE MATERIEL COMMAND
Hanscom AFB, MA 01731-3010

This technical report has been reviewed and is approved for publication.

/ Signed /	/ Signed /
GLEN MARPLE, SMSGT, USAF Contract Manager	ROBERT A. MORRIS Branch Chief

This document has been reviewed by the ESC Public Affairs Office and has been approved for release to the National Technical Information Service (NTIS).

Qualified requestors may obtain additional copies from the Defense Technical Information Center (DTIC). All others should apply to the NTIS.

If your address has changed, if you wish to be removed from the mailing list, or if the addressee is no longer employed by your organization, please notify AFRL/VSIM, 29 Randolph Rd., Hanscom AFB, MA 01731-3010. This will assist us in maintaining a current mailing list.

Do not return copies of this report unless contractual obligations or notices on a specific document require that it be returned.

REPORT DOCUMENTATION PAGE

Form Approved
OMB No. 0704-01-0188

1. REPORT DATE *(DD-MM-YYYY)*	2. REPORT TYPE	3. DATES COVERED *(From - To)*
05-12-2003	Scientific Report No. 1	30 September 2002--30 September 2003

4. TITLE AND SUBTITLE
Imaging and Forecasting of Ionospheric Structures and their System Impacts

5a. CONTRACT NUMBER
F19628-02-C-0092

5b. GRANT NUMBER

5c. PROGRAM ELEMENT NUMBER
61102F

6. AUTHORS
Bodo Reinisch, Gary Sales

5d. PROJECT NUMBER
2311

5e. TASK NUMBER
SD

5f. WORK UNIT NUMBER
AD

7. PERFORMING ORGANIZATION NAME(S) AND ADDRESS(ES)
University of Massachusetts Lowell
Center for Atmospheric Research
600 Suffolk St.
Lowell, MA 01854

8. PERFORMING ORGANIZATION REPORT NUMBER

9. SPONSORING/MONITORING AGENCY NAME(S) AND ADDRESS(ES)
Air Force Research Laboratory
29 Randolph Rd
Hanscom AFB, MA 01731-3010
Contract Manager: SMSgt Glen L. Marple

10. SPONSOR/MONITOR'S ACRONYM(S)

11. SPONSOR/MONITOR'S REPORT NUMBER(S)
AFRL-VS-HA-TR-2004-1037

12. DISTRIBUTION/AVAILABILITY STATEMENT
Approved for public release; distribution unlimited

13. SUPPLEMENTARY NOTES

14. ABSTRACT
The coordinated South American ionospheric measurement campaign, COPEX was held from October through December, 2002. Analysis of the sounder data fom the equatorial site at Cachimbo, Brazil reinforced the general understanding of the difficulty in predicting the onset of spread F on any particular night. Measurement of sporadic E formation at the magnetic field footprint in the anomaly regions provided no insight into the spread F formation problem.

RPI/IMAGE reception of groundbased VLF transmissions in space over a period of two years was used to determine the efficiency for generating whistler mode waves that propagate along the magnetic field to the satellite. These results are compared with AFRL ray tracing simulations.

Extensive analysis was carried out on the use of VLF/LF transmissions from a space platform to interact with high energy trapped electrons in the plasmasphere and scatter them so that they cannot cause damage to low earth orbiting satellites.

15. SUBJECT TERMS
Spread F, Sporadic E, Ionospheric sounding, COPEX, Equatorial irregularities, Whistler waves, VLF transmissions, Ray tracing, Radiation remediation, Trapped electrons, Wave/particle interaction, Plasmasphere, Magnetic field, HAARP, Cal/Val

16. SECURITY CLASSIFICATION OF:			17. LIMITATION OF ABSTRACT	18. NUMBER OF PAGES	19a. NAME OF RESPONSIBLE PERSON
a. REPORT	b. ABSTRACT	c. THIS PAGE			SMSgt Glen L. Marple
UNCL	UNCL	UNCL	UNL		19B. TELEPHONE NUMBER *(Include area code)* (781) 377-3151

CONTENTS

FIGURES

TABLES

1. INTRODUCTION

For the past year, the University of Massachusetts Center for Atmospheric Research (UMLCAR) has been active in a variety of areas in support of this AFRL contract entitled "IMAGING AND FORECASTING OF IONOSPHERIC STRUCTURES AND THEIR SYSTEM IMPACTS." Several of these areas are discussed briefly in this introduction and four subjects are presented in greater detail in the subsequent sections of this report. The detailed presentations are:

1. COPEX – The joint AFRL/Brazil campaign was carried out from October through December 2002. We investigated the development of spread F at the equatorial site at Cachimbo, Brazil. In particular, the correlation with the occurrence of sporadic E-layer formation at the northern and southern anomaly sites on the same magnetic meridian as Cachimbo was examined. This analysis also included the vertical motion of the F-layer during the sunset period and the height of thE-layer when spread F began.

2. VLF station monitoring in space – After detecting the presence of VLF signals from the global array of high power VLF stations with the radio plasma imager (RPI) on board the IMAGE satellite Reinisch et al., 2000), a systematic investigation of the spatial and temporal distributions of these received signals was carried out. Using the data collected over a two-year period (2002/2003) we were able to confirm the reception of these signals from the vicinity of each station and the distance and azimuthal dependence between the station location and the magnetic field line footprint of the satellite.

3. LORERS – UMLCAR has developed the concept of a low orbiting satellite that efficiently transmits low frequency electromagnetic waves in the whistler mode that can alter the pitch angle distribution of high-energy electrons trapped in the earth's radiation belts that are potentially damaging to satellites in orbits below 1000 km. This section includes a description of the proposed technique and an estimate of the required capabilities of such a system. UMLCAR is also part of the team contributing to the proposed DSX satellite for transmitting VLF radio waves in space.

4. SSUSI/SSULI – CAL/VAL – This project involves the establishment of a substantial database from a global network of digisondes to support the evaluation of the SSUSI/SSULI measurements from a DMSP satellite launched in October 2003. The digisonde ground-based electron density profiles will serve as "ground truth" for the satellite-borne UV optical measurements of electron density. UMLCAR has established a global network of 36 sounding systems as well as the data storage and processing capabilities to handle the large number of data sources. Several "dry runs" to test the UMLCAR database system have been held while the project waited for the satellite launch.

In addition to the major efforts listed above, several other areas of activity are addressed in this annual report. As part of UMLCAR's global ionospheric effort we continue to support the USAF/DISS network, providing data archiving, updating software, servicing electronic failures, and providing general support to the operators and users of the system.

Besides providing general support to the HAARP digisonde (DPS) over the past year, UMLCAR cooperated with AFRL on a campaign during the last week of August 2003. This campaign was held to develop new diagnostic techniques using the HAARP transmitter, the digisonde, and the all-sky imager as part of a coordinated measurement program. Unfortunately, the weather (generally cloudy skies) interfered with the all-sky photometer observations and it could not contribute to the program at that time. The following objectives were pursued:

1. Control the HAARP transmitter from the DPS using fixed-frequency operation, and receive high power echoes with the four DPS receive antennas.

2. Transmit pulses with DPS-HAARP at ~7.95 MHz and search for reflected signals from satellites passing overhead at 1000 km altitude.

3. Transmit pulses with DPS-HAARP at ~7.95 MHz and search for echoes from meteors at 85 to 115 km altitude.

4. Transmit using HAARP at ~4.5 MHz (CW) to heat the F region and at the same time make digisonde sky maps using 4.5 MHz pulsed DPS-HAARP transmissions to observe effect of heating. These measurements were to be compared with the optical observations.

5. Compare sky maps obtained with DPS-HAARP transmissions and with DPS-only transmission.

Results from this campaign will be discussed in future reports. Finally, new methods were developed for the real-time analysis and display of F region drift velocities V_z, V_{north}, and V_{east}. These real time digisonde outputs can become an important input for the Air Force's space weather prediction effort. In addition, new software for the post analysis of digisonde drift measurements, the "Drift Browser," is under development. A future technical report will be dedicated to the description of the digisonde drift measurement and analysis techniques.

2. COPEX

2.1 Introduction

The conjugate point equatorial experiment (COPEX), organized by the Instituto Nacional de Pesquisas Espaciais (INPE), Brasil with the support of AFRL and UMLCAR, was conducted between 1 October and 9 December 2002. It involved a coordinated set of measurements across the South American continent from Jicamarca in the west to Sao Louis in the east, primarily along the magnetic equatorial region. In this report, we discuss digisonde data from the three Brazilian sites: Boa Vista (Lat = 2.8°, Long = 299.3°), Cachimbo (Lat = -9.5°, Long = 305.2°) and Campo Grande (Lat = -20.5°, Long = 305.0°). A sounder was operated at each of the three sites on a five-minute schedule during the entire campaign. These three sites (see Figure 1) were selected because they lie along almost the same magnetic meridian with Cachimbo near the

magnetic equator (dip angle = -3.91°), Boa Vista to the north of the magnetic equator at approximately + 22 degrees dip angle (equatorial anomaly region) and Campo Grande to the south of Cachimbo in the southern anomaly region (dip = -22°). The local time at Cachimbo and Campo Grande is –03h 40min from UT and Boa Vista is –04h 02min.

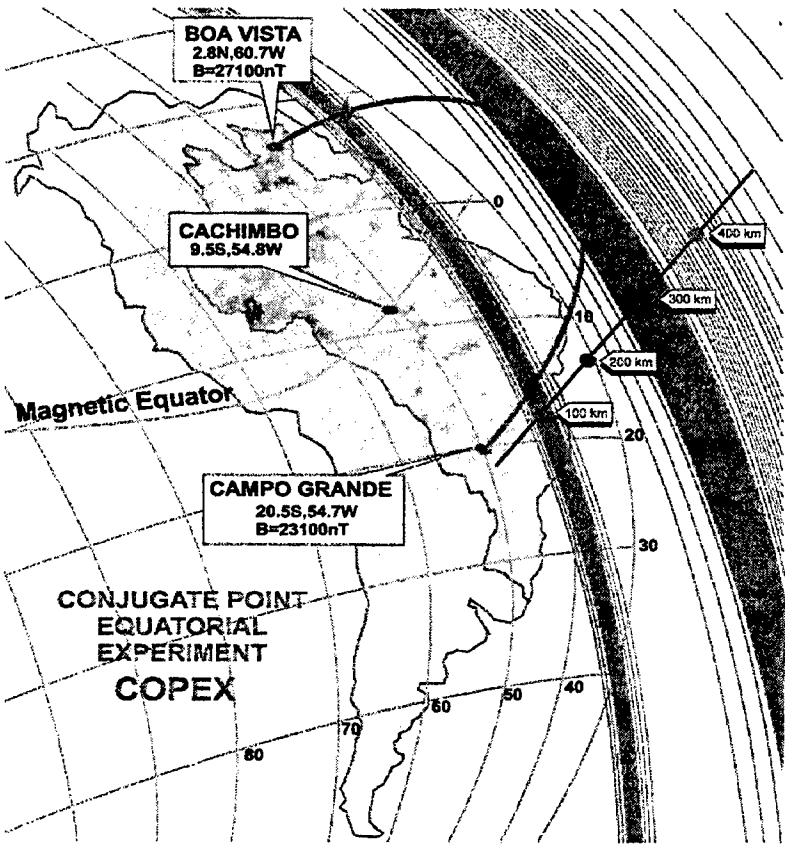

Figure 1. Map of South America and the COPEX Digisondes

One of the primary goals of this campaign was to determine how the presence of sporadic E (Es) at either anomaly location affects the generation of spread F at Cachimbo. The two anomaly sites were selected so that the magnetic field line over Cachimbo at 350 km passed over the northern and southern sounder sites at E region altitude (≈ 100 km). The assumption being that the higher conductivity resulting from the presence of Es at either end of the field line might short out the electric field, preventing the F-layer at Cachimbo from moving to a higher altitude regime that better supports the growth of F region instabilities. The development of F region instabilities occurs near the bottom of the F-layer where the electron density height gradient is largest (Kelley, 1989). The other important factor in the growth of the Rayleigh-Taylor (R-T) instabilities is the electron-neutral collision frequency. At higher altitudes, the collision frequency decreases exponentially resulting in the increase of the R-T growth rate. There the F-layer is more likely to become unstable and develop bottom side equatorial spread F and large scale bubbles.

Since the development of F region instabilities typically occurs around sunset, this report concentrates on the period from 2000 UT through to 24 UT (from approximately 90 minutes before F region sunset to 90 minutes after sunset) using the measured electron density profiles and vertical and horizontal plasma drift velocities. The F region sunset variation at Cachimbo during COPEX is shown in Figure 2. The F region sunset was calculated by adding 64 minutes to ground sunset time. The delayed sunset (corresponding to a solar zenith angle of 108°) accounts for the fact that solar UV, responsible for maintaining the lower F region, can penetrate the earth's atmosphere at least above the 30 km ozone region.

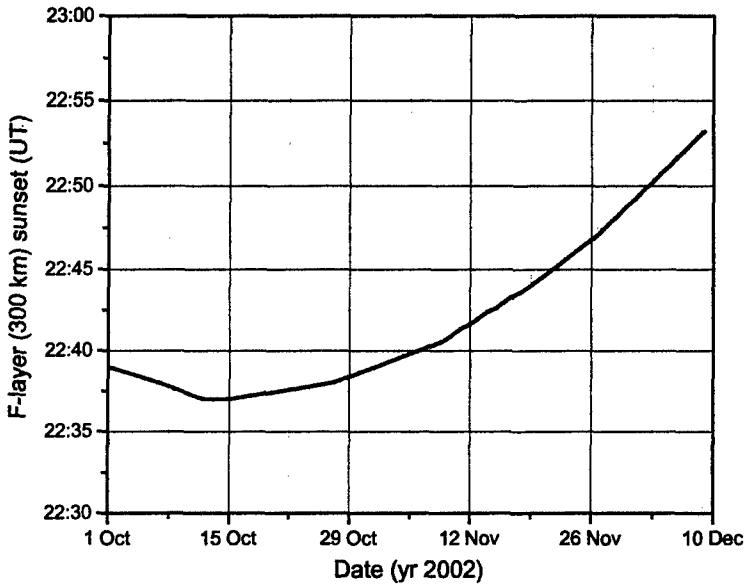

Figure 2. Sunset for the F-Layer (300 km altitude) at Cachimbo.

Spread F occurred on 64 out of the 70 nights that the three sounders operated during the COPEX campaign. There were only six nights with no spread F development. Our analysis attempted to answer the question as to what the differences were during these six nights that inhibited the sustained growth of ionospheric irregularities. Section 2.2 presents the basic analytical tools developed for this investigation. In Section 2.3, the issue of the presence and influence of Es at the anomaly sites is examined. In Section 2.4 the question of the effect of the vertical and horizontal plasma motions at Cachimbo is discussed.

2.2 Analytical Method

The early formation of bottom-side F-layer irregularities had to be defined beyond the usual spread F indices that are used in ionograms scaling. The reason for this was that at the earliest stages of irregularity formation, the digisonde system often detected the presence of structures very near the vertical trace as thE-layer begins to deform under the

influence of the R-T instability growth. These structures do not show up as classical spread F until a later time when the irregularities are more developed along the vertical or other traces on the ionograms. A clear example of these early-time phenomena is shown in a sequence of ionograms in Figure 3.

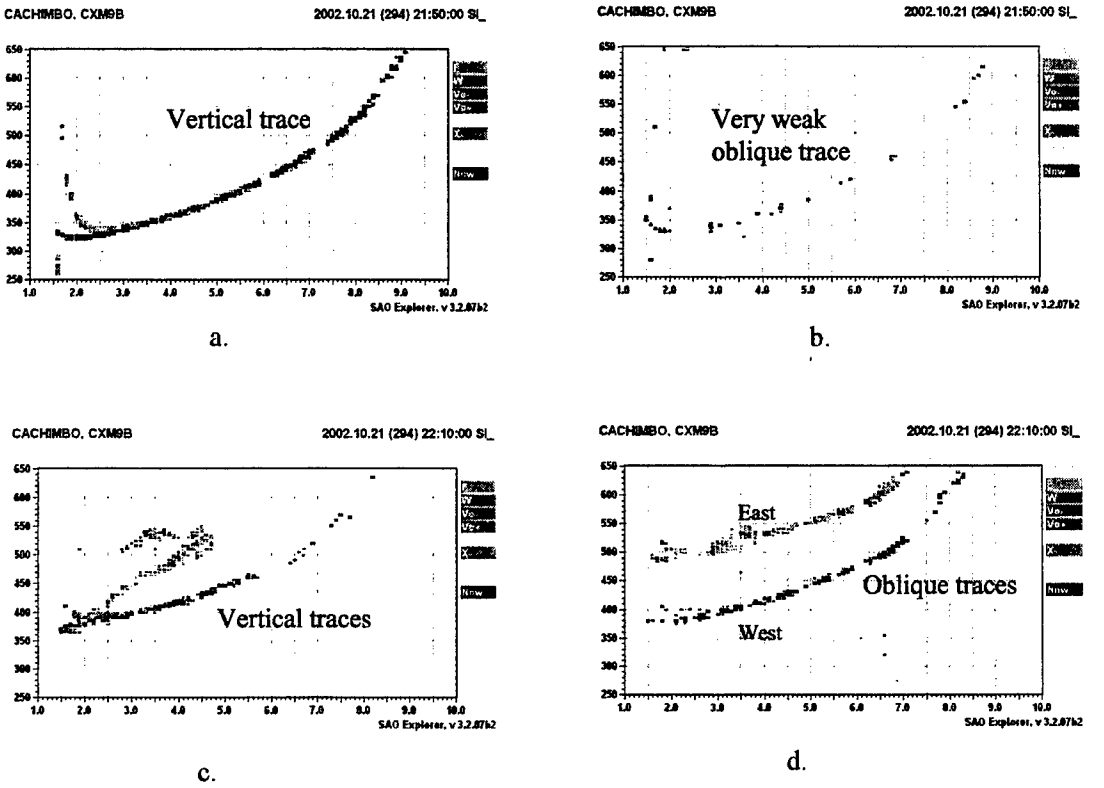

Figure 3. Cachimbo Ionograms 21 October 2002.
a. 2150 UT, Vertical Echoes b. 2150 UT, Weak Non-Vertical Echoes
c. 2210 UT, Vertical Echoes), d. 2210 UT, Non-Vertical Echoes East and West of Cachimbo

In this example, the non-vertical traces, almost coincident with the vertical trace, appear around 2200 UT. This issue is discussed in more detail later in the report. At this point, the example is used as an illustration of the "activity index" developed for this analysis. Figure 4 shows the "directogram" (Reinisch et al., 2003) derived from the ionograms in the period from 2100 UT through 2300 UT for 21 October 2002. The directogram shows the direction (east/west) and distance to the reflection points of the non-vertical echoes. Each line in the directogram represents one ionogram, spaced 5 minutes apart during COPEX.

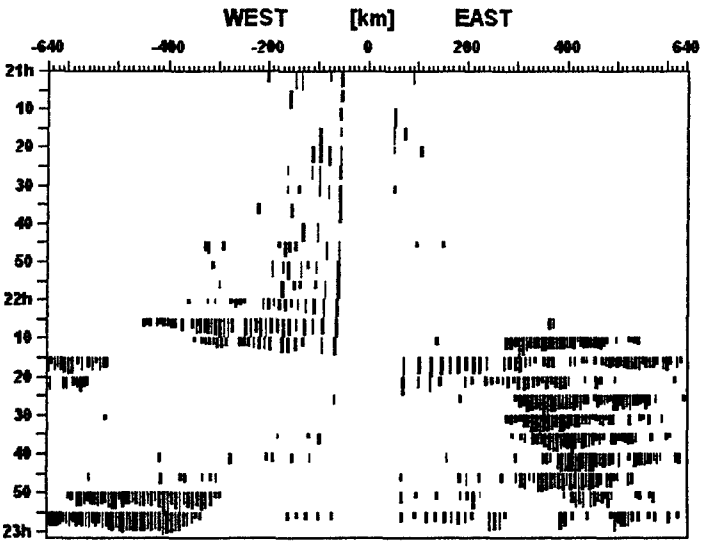

Figure 4. Directogram: Cachimbo, 21 October 2002, 2100 – 2300 UT

The strong now vertical echoes begin at 2205 UT in the F region to the west of Cachimbo. At 2210 UT, an additional strong echo appears in the east. These early traces represent the beginning of a bubble structure nearly overhead from Cachimbo. Tracing the early phases of the growth of these medium scale (order of 100 km) instabilities is possible using the sequence of ionograms as illustrated in Figure 3. This approach will be used in our future research effort.

The activity index (AI) developed for this study is the logarithm (base 10) of the sum of the directogram amplitudes for each ionogram (horizontally across the directogram). The index typically varies from of the order of 2 (100) to a maximum of less than 4 (10,000). Figure 2-5 shows the AI variation for the week of 1 Oct. through 7 Oct. 2002 at Cachimbo for the hours from 2100 UT to 2355 UT.

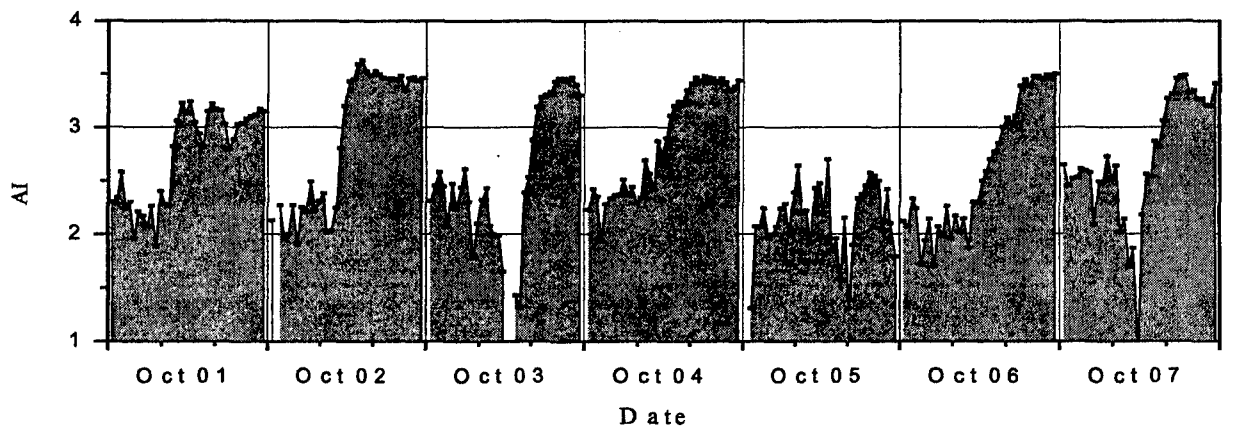

Figure 5. Activity Index for the Week Beginning 1 October 2002. Each Daily Panel Runs From 2100 UT to 2400UT.

The "noise" level of AI, before F-layer activity begins, is approximately 2 as seen in Figure 5. When the instabilities growth begins, AI rapidly increases to a level greater than 3. For the rest of this paper, the onset time of spread conditions was set at the time when AI first exceeds 3. On Oct. 5, AI never reached 3 and this day was designated as a quiet (no activity) day. As stated earlier, there were six such days out of the seventy COPEX days. For the 64 active days the "onset" time (AI > 3) varied considerably as is shown in Figure 6. The reference time used here was the F-layer sunset time. The median time delay was –10 minutes, i.e., 10 minutes before sunset. The other statistics are shown in the legend but the important one is that on 81 percent of the days, spread F activity began before [sunset + 10 minutes]. Only 5 percent of the days (4 days) were late starters, i.e., onset began after [sunset + 30 minutes].

Two reference times are used to organize the equatorial phenomena. The first is F-layer sunset that varies during COPEX as shown in Figure 2. The second time reference used here refers to what appears to be the very first indication of F-layer changes during this sunset period. Typical examples of these changes are shown in Figure 2-3d. These are designated as "satellite" traces that appear at different range than the vertical trace. As is discussed in greater detail later, these satellite

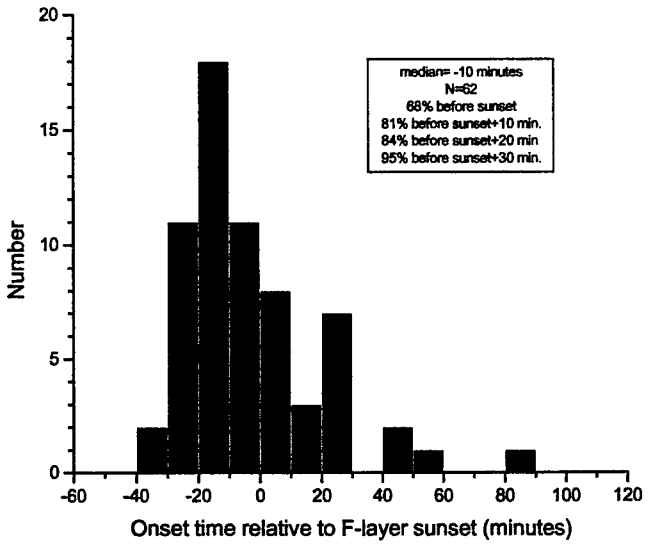

Figure 6. Distribution of F-Layer Instability Onset Times for Cachimbo.

traces are recognized as resulting from the early of the bottom of the F-layer and the first observation of these traces is used as a reference time in this analysis. When this is done for the AI onset, the results are shown in Figure 7. Here, the satellite trace (ST) start time is used as the reference time for AI onset. The median time difference was 15 minutes, however on 36 percent of the 64 active nights the layer instability began within 10 minutes of the appearance of these satellite traces. The structure of the F-layer bottom and the development of the satellite traces are discussed in greater detail below.

Finally, this analysis examined the presence of sporadic E traces on the vertical ionograms at Boa Vista and Campo Grande and their effect on the growth of the

instabilities at Cachimbo. Here, the automatic scaling of foEs was used as the measure of the presence of sporadic E.

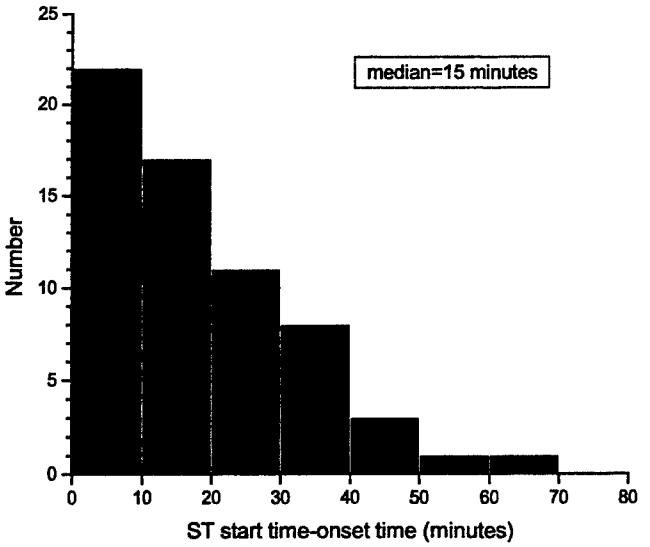

Figure 7. The Instability Onset Time Relative to the Appearance of Satellite Traces (ST) on the Ionograms From Cachimbo During COPEX.

2.3 Effect of Sporadic E on the Development of F-layer Instabilities on the Magnetic Equator

The COPEX campaign provided the unique opportunity to investigate the effect of the presence of sporadic E on either end of the magnetic field line passing over an equatorial station. The value of foEs in our analysis used at any time is the greater of the two measurements at Boa Vista and Campo Grande. Figure 8 shows the distribution of foEs at several times during the early sunset period on 68 days. On 1 and 2 October, both anomaly sites were not operating. The first two panels (a. and b.) are at 2200 UT and 2215 UT, respectively. For both these panels (before F layer sunset) sporadic E was not detected at either site on 36 percent of the nights. On the remaining 50 nights, the median foEs decreased from 3.0 MHz to 2.75 MHz in the 15 minutes from 2200 UT to 2215 UT (40 minutes and 25 minutes before the average F-layer sunset, respectively). Panel c., at the time of spread F onset is at a later time, on the average some 10 minutes before sunset and the number of days where no Es were detected increased to 50 percent, though the median foEs on the remaining nights remained at around 2.9 MHz. Finally, the distribution of foEs at the time thE-layer over Cachimbo was rising at the maximum rate ($V_{z,max}$) is

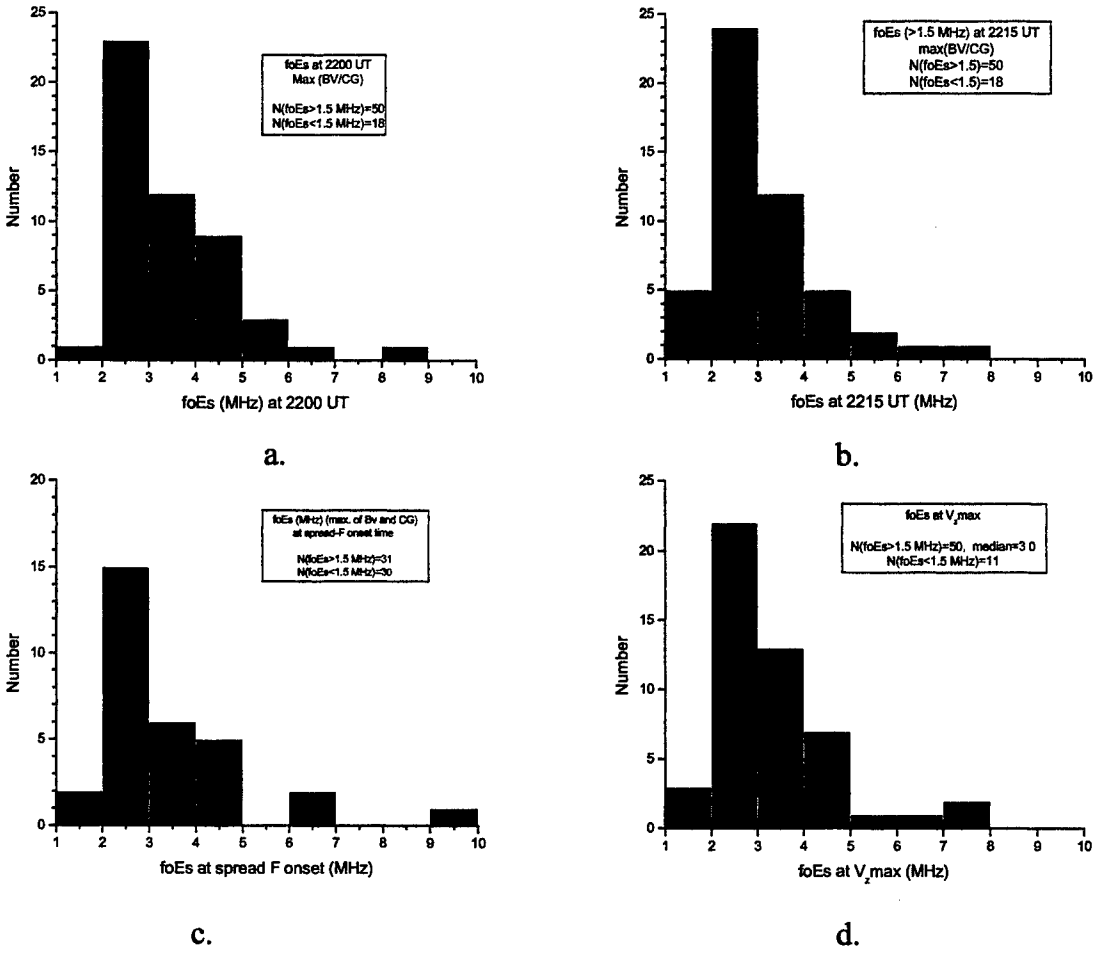

Figure 8. Distribution of foEs at Several Times During Sunset Period. a. at 2200 UT, b. at 2215 UT, c. at F-layer Instability Onset Time, d. at Time of Maximum Vertical Velocity at Cachimbo on the Magnetic Equator.

shown in Panel d. Referring to Figure 9, the median time for $V_{z,\,max}$ was 2210 UT, falling between the times used in Figures 8a and b. At the time of $V_{z,max}$ no Es was detected on only 11 days (compared to 18 days at 2200 and 2215 UT). Using the $V_{z,max}$ distribution as a reference for sporadic E suffers from the problem that this event does not occur at a specific time and that on some fraction of the observed days it occurs before 2200 UT when sporadic E is more likely.

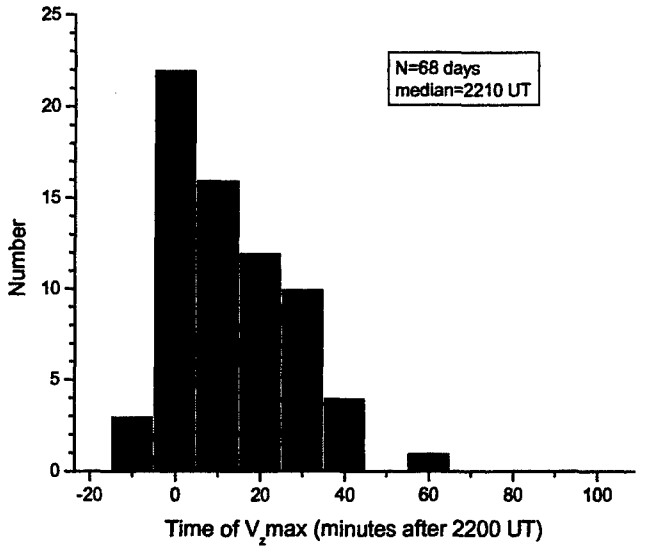

Figure 9. Distribution of the Time of Maximum Vertical Velocity at Cachimbo.

Before examining foEs on the six quiet days, the observed range of foEs on the active days was from no detectable Es (foEs < 1.5 MHz) to a maximum of from 6 to 10 MHz (see any of the distributions in Figure 8), depending on the time of the measurement. Given this range of values of foEs on the active days certainly makes it difficult to understand the role of sporadic E, if any, to control the development of spread F on that field line above the magnetic equator. With this overall view of sporadic E variation during the active evenings of COPEX, the distribution of foEs on the quiet days can also be compared to the larger database of active days.

Table 1. foEs on Quiet Days

Date	foEs (2200 UT)	foEs (2215 UT)	Time of $V_{z,max}$	foEs (at time of $V_{z,max}$)
Oct. 5, 2002	2.4 MHz	2.3 MHz	2200 UT	2.4 MHz
Oct. 14, 2002	4.7	7.9	2210	7.7
Oct. 16, 2002	3.9	2.6	2205	2.6
Oct. 24, 2002	3.4	3.8	2155	2.4
Oct. 31, 2002	3.3	3.9	2200	3.3
Nov. 2, 2002	> 1.5	4.3	2200	> 1.5

On these six quiet days the max foEs distribution at the same times as for the active day distributions is very similar to the ones for the active days, ranging from below 1.5 MHz up to 7.9 MHz.

The conclusion then is that the presence or lack of sporadic E at the feet of the magnetic field line plays no role in inhibiting or encouraging the development of equatorial spread F at the magnetic equator.

2.4 Vertical and Horizontal Plasma Drift in Relation to the Development of Spread F at the Magnetic Equator

In between ionograms at Cachimbo, the digisonde was operated in the "drift" mode, measuring the F region plasma drift velocity every five minutes. The data presented here show the smoothed Cartesian components of the drift velocity. The running average is over a twenty-minute period (±10 minutes) for the vertical, east/west and north/south components. Figure 10 shows the typical diurnal variation of the three drift components for two consecutive days in October.

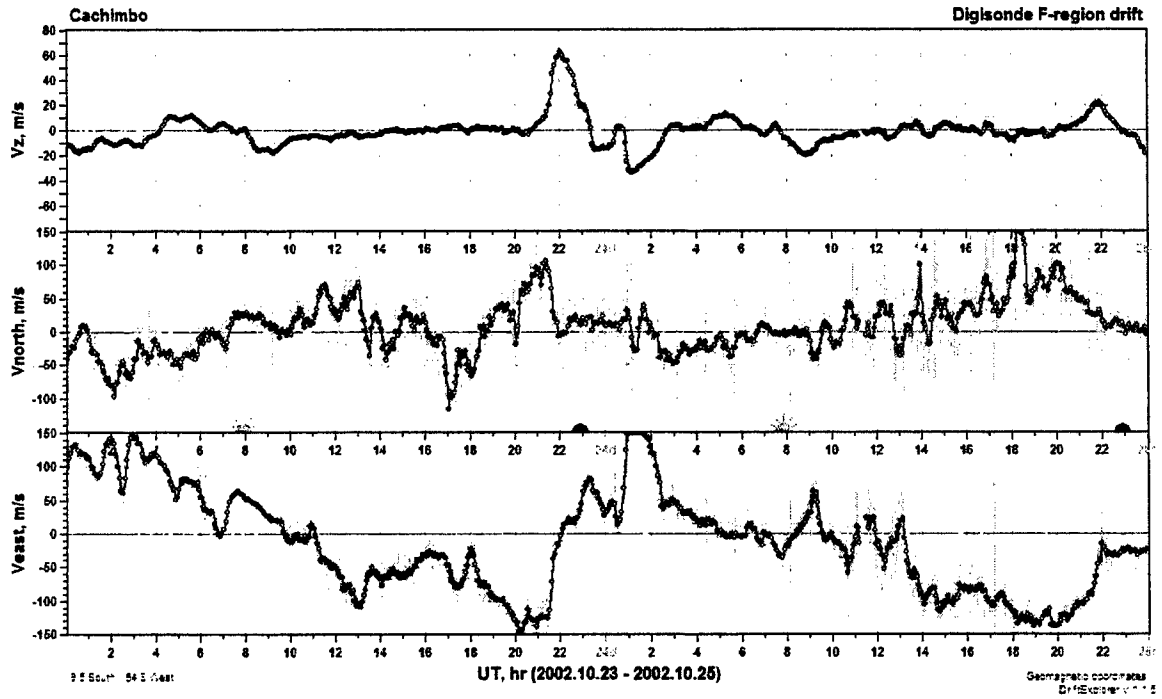

Figure 10. Typical Diurnal Variation (23-24 October 2002) of the F-Region Drift Velocity Components as Measured by the Digisonde at Cachimbo. F region Sunrise (08 UT) and Sunset (23 UT) are Indicated by Half Circles in the Middle Panel.

Of particular interest is the increased vertical velocity that occurs shortly before sunset at 2200 UT on 23 October. This increase has been characterized in many prior publications as the "pre-reversal enhancement." This reversal refers to the relatively rapid change in the direction of the zonal drift component from west to east that coincides with this increase in the vertical velocity. The vertical velocity begins to increase, reaches a peak and decreases, on the average, over a period of about 2 hours, all before F-layer sunset. The two parameters derived to characterize this behavior are the time of maximum velocity, relative to F-layer sunset, and the magnitude of the maximum velocity. The distribution of these parameters is shown in Figure 11. The median time of the peak vertical velocity was –33 minutes relative to F-layer sunset for the active days. The median vertical velocity at Cachimbo was 52.8 m/s, again on the active days. In both panels of Figure 11, the quiet day distributions of the same parameters are also shown. At the time of the peak velocity, the two distributions are indistinguishable, considering the

small size of the quiet day population. However, for the magnitude of the vertical velocity, clearly the quiet day numbers lie near the lower end of the active day distribution. One conclusion that can be drawn is that when the vertical drift velocity exceeds 45 m/s, spread F always developed. On days when the vertical velocities is less than 45 m/s, there is a 67 percent probability of the night being active and 33 percent of being a quiet night.

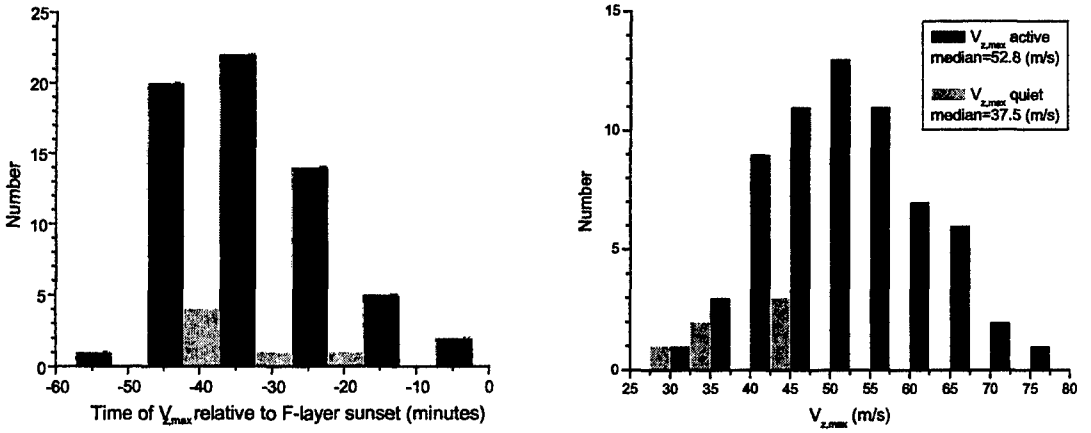

a. b.

Figure 11. Vertical Drift Velocity Distributions at Cachimbo.
a. Time of Maximum Velocity Relative to F-layer Sunset
b. Magnitude of Maximum Vertical Velocity

The vertical velocity increase during the pre-reversal enhancement certainly drives the F-layer to greater heights. Here the auto-scaled h_{min} (the minimum F-layer virtual height) was used as a measure of the height of the F-layer bottom where instabilities are most likely to develop initially. Figure 12 shows the distribution of h_{min} at the time of spread F onset for the active nights and at ten minutes before sunset (median time of spread F onset) for the quiet days. The median height of the bottom of the F-layer reached at onset time was 395 km with a spread of about ±80 km for the active nights. The distribution for the quiet nights is not significantly different, considering the small sample size.

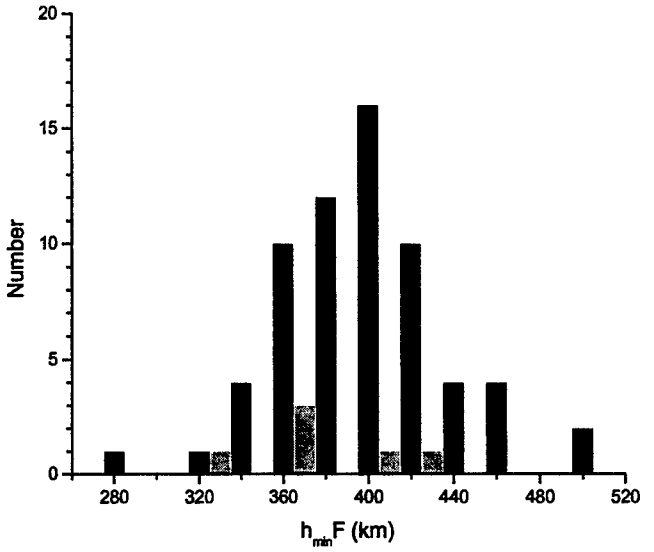

Figure 12. Distribution of Minimum F-layer Heights hminF at Time of Spread F Onset (black) and for Quiet Days (gray).

2.5 Conclusions

It is not easy to make a distinction between quiet and active spread F nights, based on the COPEX campaign data. The magnitude of the vertical velocity does indicate that the higher speeds do produce spread F, however lower speeds do not guarantee a quiet night. The height to which the bottom of the F-layer has risen does not significantly affect the probability of spread F development. The crucial question then is what are the controlling factors or does it depend only on the presence of a trigger mechanism, e.g., gravity waves. Future efforts will concentrate on several areas:

a. The east/west and north/south drift velocity components as indicators of thE-layer behavior at the onset time.
b. The formation of satellite traces as an early indicator of the F-layer instability.
c. Electron density gradients near the bottom of the F-layer.

3. MONITORING OF GROUND-BASED VLF TRANSMITTERS IN SPACE

3.1 Introduction

Approximately six months ago it was recognized that the RPI receiving system aboard the IMAGE satellite was receiving transmissions from several ground-based VLF transmitters, usually when the satellite was on or near the magnetic flux tube centered on the VLF station. This configuration is illustrated in Figure 13.

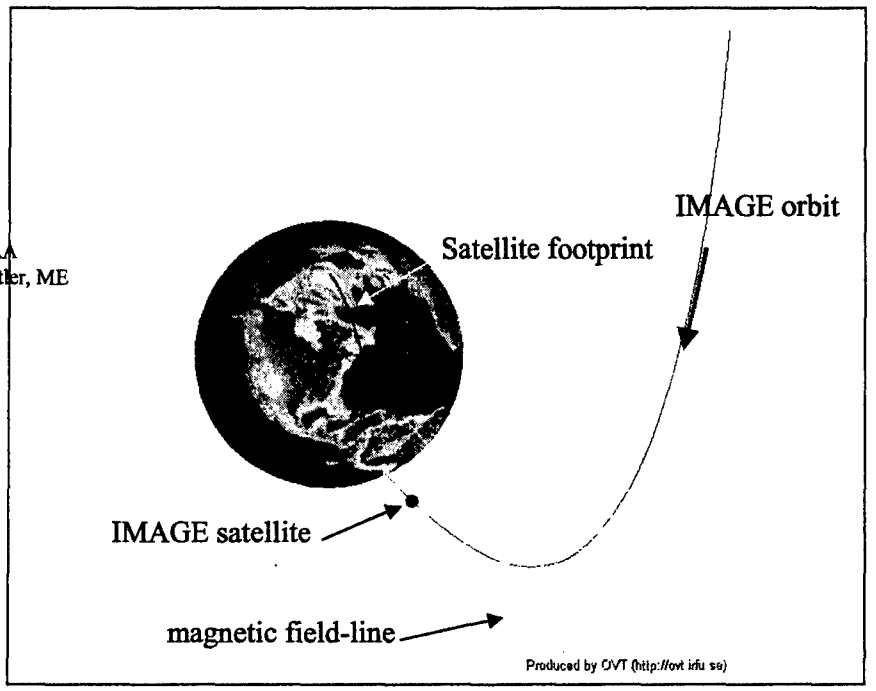

Figure 13. Illustration of the Relationship Between the IMAGE/RPI Satellite and the Magnetic Footprint in the Vicinity of the VLF Transmitter (NAA) at Cutler, Maine.

Figure 14 shows the relationship between the satellite's magnetic field footprint and the VLF station, NAA, at Cutler, ME. The illustrated track begins at 1400 UT on 4 April 2001 and sweeps past the VLF site at 1544 UT. During this period, the signals from the transmitter were received by RPI on the IMAGE satellite. These observations were made when RPI was operating in the dynamic spectrogram mode stepping from 3 kHz to 1 MHz in increments of 400 Hz. The example a spectrogram in Figure 15 shows several natural noise sources and the VLF station, NLK located in the state of Washington. For the VLF band observed by RPI, Table 2 lists the characteristics of the seven most powerful VLF transmitters, in order of increasing frequency.

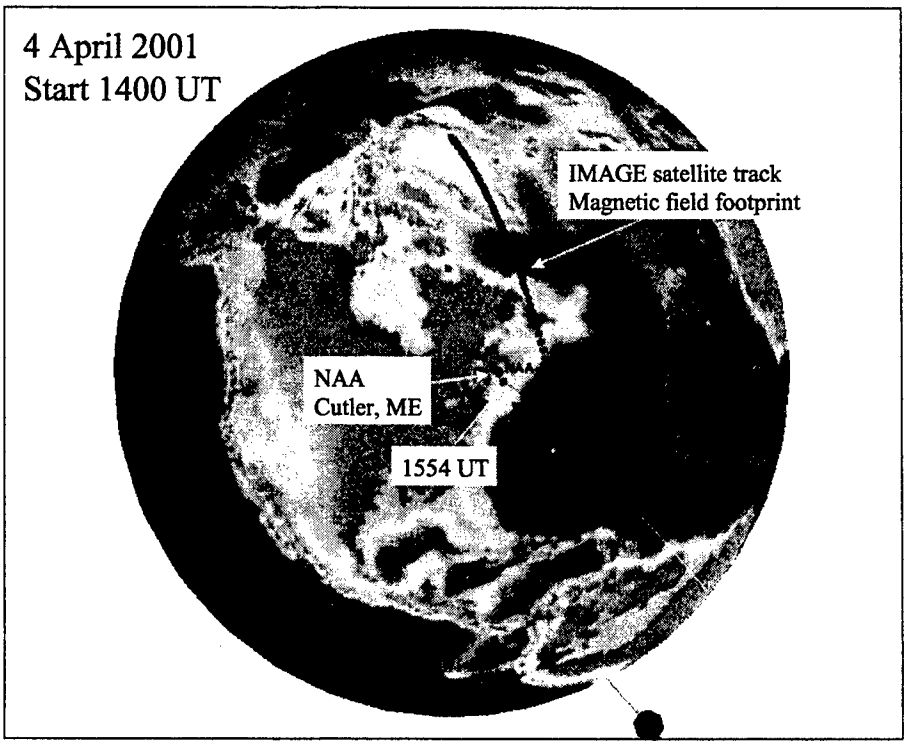

Figure 14. Illustration of the Satellite Ground Track Following the Magnetic Field Line Through the Satellite Location.

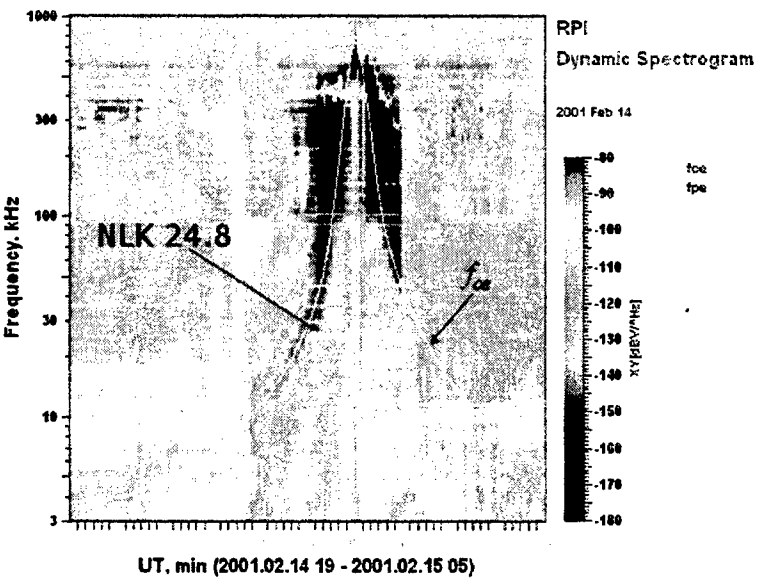

Figure 15. Dynamic Spectra Measured by RPI/IMAGE on 14 February 2001, 1900 UT Through 15 February 2001, 0500 UT. The Horizontal indicated trace between 0000 UT and 0100 UT at 24.8 kHz represents the received signal from NLK.

Table 2. Location and Characteristics of the Seven Most Powerful VLF Stations Observed by RPI.

Freq. (kHz)	Station Identifier	Power (kW)	Location	Geographic Lat.	Geographic Long.	L-shell
19.8	NWC	1000	Exmouth, NWC, Australia	21.8 S	114.1 E	1.41
20.9	HWU	1000	Rosnay, France	46.7 N	1.3 E	1.79
21.4	NPM	566	Laulaulie, Hawaii	21.4 N	201.9 E	1.45
23.4	DHO	500	Randerfehn, Germany	51.2 N	7.9 E	2.15
24.0	NAA	1000	Cutler, Maine, USA	44.7 N	292.7 E	2.87
24.8	NLK	250	Arlington, WA, USA	48.2 N	239.0 E	2.89
25.2	NML	500	La Moure, ND, USA	46.4 N	261.7 E	3.26

3.2 Data Collection and Analysis

For all the RPI/IMAGE orbits during the two-year period 2001 - 2002, the received signal amplitude from these seven VLF transmission transmitters were collected whenever the satellite was within $L < 5$, that is, essentially inside the Earth's plasmasphere. Results for the two-year period are summarized in Figure 16 for the VLF transmitter NML (25.2 kHz) located in North Dakota, for both night and day. In this figure, the received signal strength (nV/m) is plotted at the location of the footprint of the magnetic field line passing through the satellite position at the time of each dynamic spectrum measurement. The signals received closest to the stations are the strongest, though they show very little decrease with distance from the VLF transmitter until a distance of more than several thousand kilometers is reached.

The model considered here for the propagation of these signals to the satellite involves several separate processes. First, the transmitted wave propagates from the station inside the earth/ionosphere wave guide. Then at each point along the wave guide, a fraction of the energy leaks out from the upper bound (ionosphere). Penetration of the ionosphere by low-frequency waves can happen only in the whistler mode. Then these whistler mode waves propagate essentially along the Earth's magnetic field line passing through the penetration point. When the penetrating wave reaches sufficiently high altitude, then the signal, free from the ionosphere, continues propagating along the field line until it reaches the satellite.

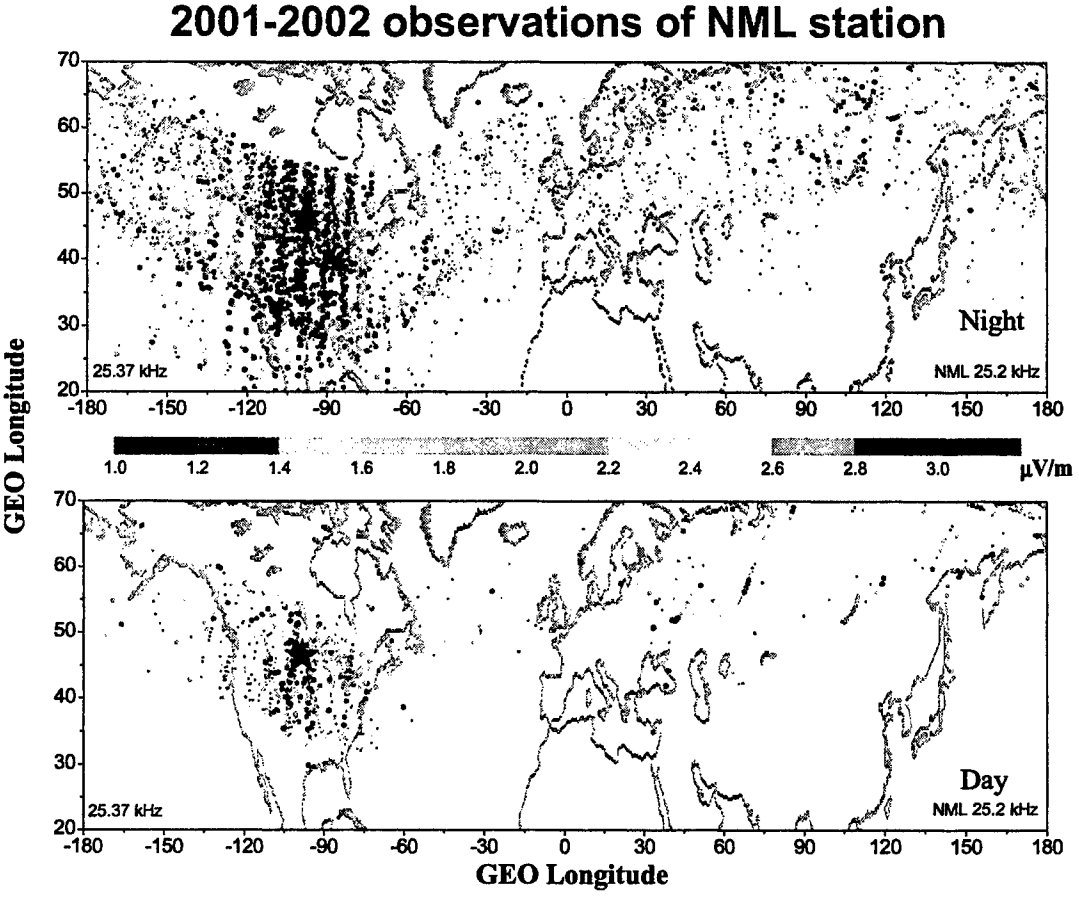

Figure 16. Geographic Distribution of Received Signal Strength for NML (24.8 kHz), a. Night, b. Day

The goal of this study is to confirm the complex propagation model by comparing received signal strengths with the calculations using wave guide propagation models, ionospheric penetration models, and then using ray tracing up to the satellite. The RPI/IMAGE measurements show a distinct difference if the observations are made in the day or the nighttime. This is to be expected since the waveguide models always show a significant increase in losses in the daytime. However, in both situations, day and night, there appears to be very little decrease in the received signal strength as the distance from the penetration point to the VLF station increases. The VLF waveguide models always predict a steady 3 or 6 dB/Mm signal attenuation inside the waveguide. To investigate this discrepancy, the characters of the received signal strength are shown in the histogram (Figure 17).

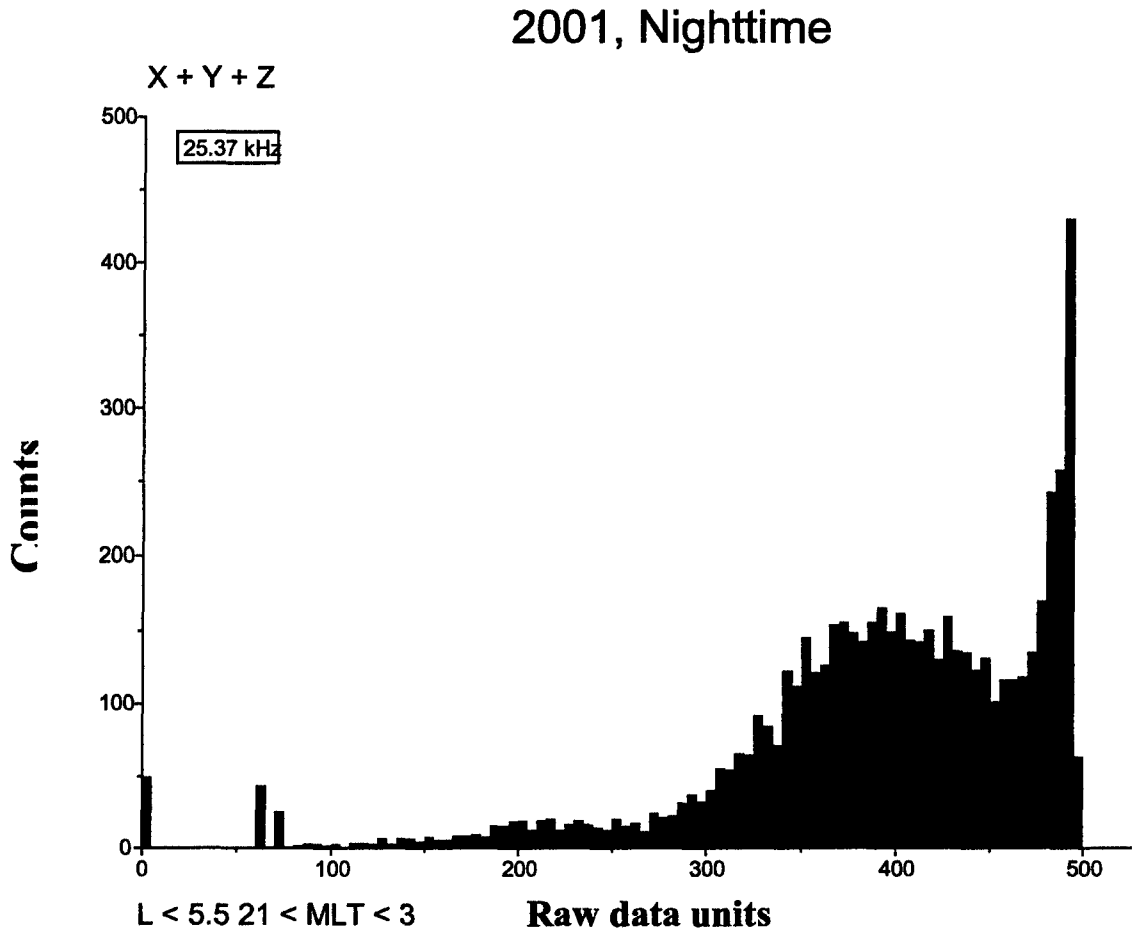

Figure 17. Distribution of Received Signal Amplitude From the VLF Transmitter, NML.

The peak of the distribution close to the maximum possible amplitude of 500 (arbitrary units) reveals a saturation effect. The problem has been analyzed to be the result of the high RPI receiver gain that was set to a level required to measure naturally occurring noise signals. This required high receiver gain settings, too high, however, for the strong VLF signals arriving at the satellite, even considering the three-stage propagation process.

3.3 Conclusions

The strong saturation of the received VLF signals has prevented quantitative analysis of the various components of the propagation model. This problem will be rectified using a special program up-loaded to the IMAGE satellite, where for several months the dynamic spectrograph mode will be operated sequentially with four low-gain settings in order to determine the best gain settings for the VLF monitoring experiments. These new data will be shared with the AFRL group interested in modeling the propagation process.

4. LOW-EARTH ORBIT RELATIVISTIC ELECTRON REMEDIATION SYSTEM (LORERS)

The objective of this project is to investigate the possibility of developing a space-borne transmitter that radiates whistler mode waves in order to protect low-earth orbit (LEO) satellites from damage by trapped relativistic (high energy) electrons, generated naturally or by any other mechanism. These whistler waves can interact with the trapped relativistic electrons in the radiation belts and reduce the pitch angles of these electrons so that they ultimately precipitate into the atmosphere, thereby doing no harm to LEO assets. The advantage of using the whistler waves is that they are energy selective, targeting only harmful electrons and they are energy efficient because they only change the pitch angle and do not need to reduce the high energy of these particles. Harmful electrons are those high-energy electrons that would normally mirror at or below the LEO orbits.

Distinct from the conventional wisdoms, which suggest putting the transmitter into a mid-earth orbit (MEO) in the equatorial plane, LORERS proposes to put the transmitter into a high-inclination low-earth orbit, as shown in Figure 18. With this configuration, the LORERS transmitter is much cheaper to launch. The question remains as to whether it is power efficient. This is the major subject in our investigation.

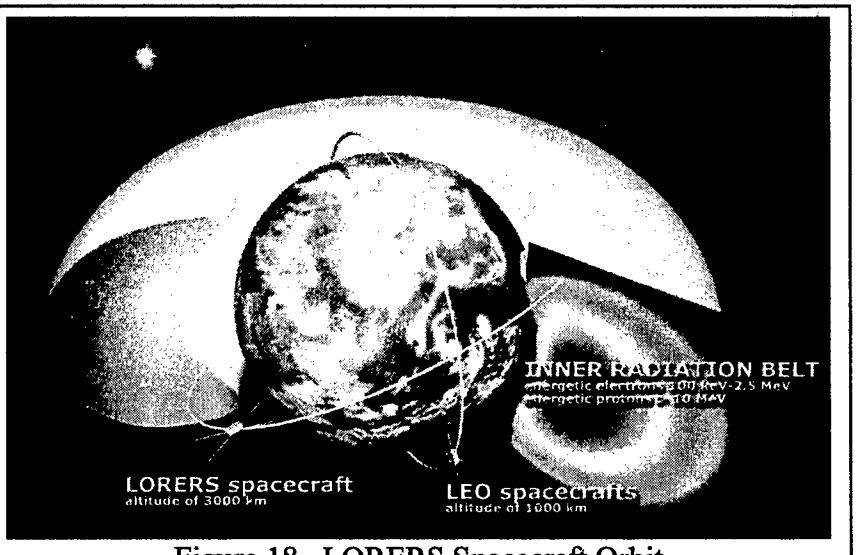

Figure 18. LORERS Spacecraft Orbit

The LORERS, will be placed in an orbit about 2000 km above the LEO satellites. The orbit inclination is such that it passes through the feet of the magnetic field lines of the radiation belts.

As shown in Figure 19, the transmitter selects a specific frequency range that resonates with the harmful electrons (upper-left panel). After the transmitter passes through a region, the region is free of relativistic electrons up to 1000 km above the LEO satellites that the LORERS is protecting (upper-right panel). When the LORERS moves away to clean other regions the natural diffusion processes will continuously feed the region with

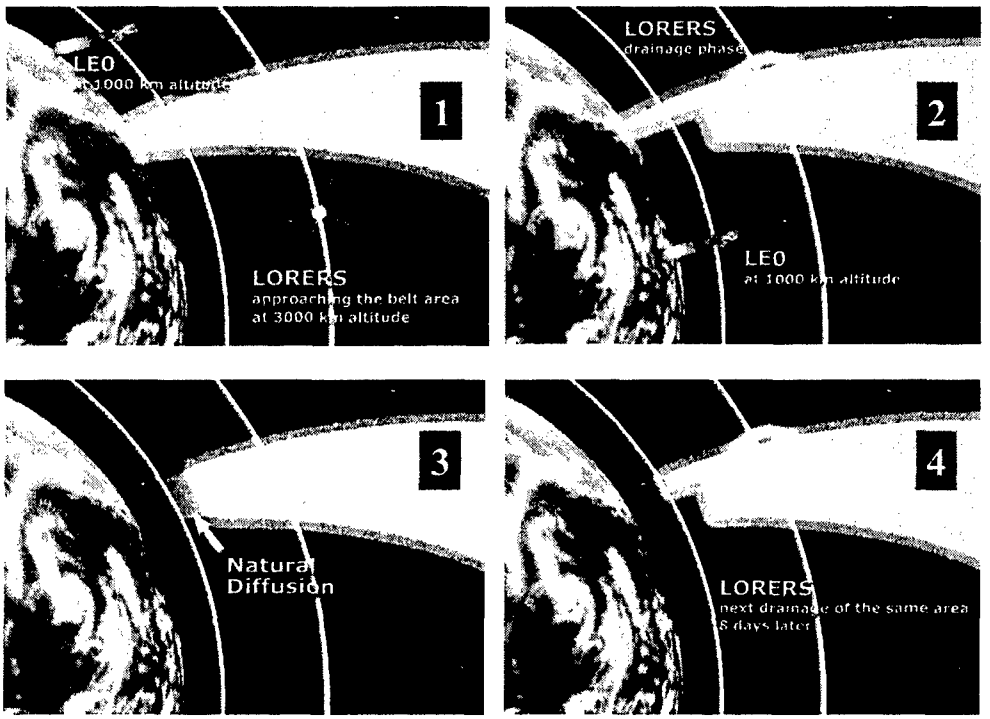

Figure 19. LORERS Cleaning Process

new harmful electrons (lower-left panel). The LORERS revisits the same region before the harmful electrons can reach the LEO orbit (lower-right panel).

LORERS is most energy efficient because it targets only the harmful electron population. The mirror effect of the Earth's magnetic field causes most particles to bounce back-and-forth across the equatorial region. Figure 20 shows the distribution of the mirror points of the radiation belt particles as functions of latitude for different L-values, normalized by their equatorial values. It is clear that less than 10 percent of the particles are actually harmful to the LEO satellites. In other words, LORERS needs to only do work on 10 percent of the total population on a field line. The other 90 percent of the work will be done by natural diffusion and will be removed at later times. The LEO assets can have a safe environment nearly immediately, but complete cleaning of the whole radiation belt lasts a long time. The cleaning process spreads in time. In contrast, the conventional equatorial cleaning scheme cleans the whole radiation belt progressively. In order to clean in a rapid and meaningful pace, a much larger transmitter power is required and after the cleaning, the transmitter in its orbit is of little use.

One disadvantage for a low-orbiting LORERS transmitter is the so-called short "in-tune" time during which the wave and resonating particles interact. We investigated this problem during the year.

Equation 1 shows the phase relation between the wave and a particle,

$$R(s) = \omega - \frac{n|\Omega_{ce}(s)|}{\gamma} - k(s)v_{\parallel}(s)\cos\theta_s \qquad (1)$$

where s is the distance from the transmitter along the field line. When the left-hand-side of the equation, R(s), is zero, the wave and particle are in resonance. The out-of tune condition is when the phase between the wave and the particle is more than $\pm\pi/4$, or when:

$$\tau\frac{\partial R}{\partial s}\Delta s = \frac{1}{v_{\parallel}}\frac{\partial R}{\partial s}\Delta s^2 \le \frac{\pi}{2} \qquad (2)$$

where τ is the in-tune time. The actual calculation of the in-tune time for LORERS is being done numerically using a dipole magnetic field model. The pitch-angle change of a particle is proportional to the square-root of the in-tune time.

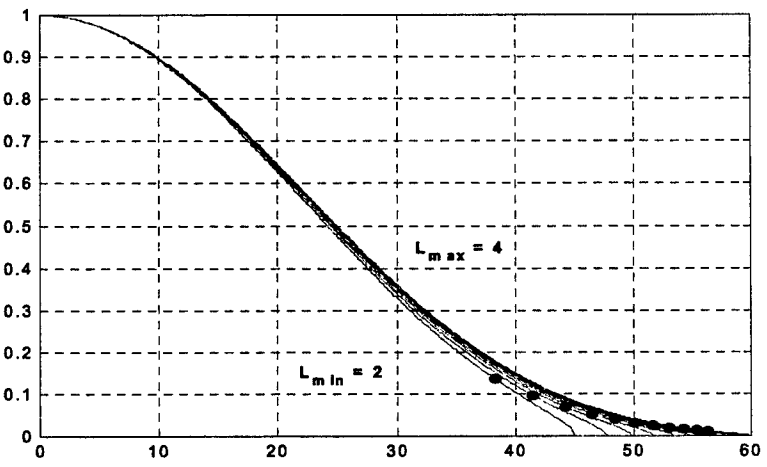

Figure 20. Distribution of Mirror Points.

The main effort during the year has been focused on the antenna/wave radiation problem. The most important issues are how much power can be radiated and what are the properties of the radiated wave. Given the relationship between the wave power/properties and the background plasma conditions, the answers to these issues ultimately determine the best location for the transmitter and the best frequency to operate at. Most of the theoretical investigations on these subjects were conducted in the late 1960s and early 1970s. We have reviewed the most important works on these subjects and found that the basic theory needs a fundamental update. Some recent work [e.g., Inan et al., 2003] was based on misunderstandings of the previous efforts. We have conducted a comprehensive theoretical investigation. The results showed that the power of the radiated wave was higher when the plasma frequencies and operating frequencies are higher than previously suggested. Given a resonant condition, this translates to a higher electron gyro frequency. Therefore, a LORERS transmitter at lower altitudes would be more efficient in terms of transmitted power.

This analysis provides the relationship between the wave amplitude and the plasma conditions and the current near the antenna. It is known that near the antenna, a high voltage on the antenna creates a plasma sheath surrounding the antenna. By reviewing the existing literature, the quantitative description of the sheath processes may be a candidate for updating. The existing theory appears not to be supported by experiments.

The only published relevant experiment [Oliver et al., 1973] indicates the theory is off by a factor of 10.

5. SSUSI AND SSULI - CAL/VAL PROJECT

5.1 Digisonde Network and DIDBase

Currently 39 digisonde stations around the world have been identified to become part of the CAL/VAL program. We have obtained permission to use the data from these stations and to change their modes of operation as required. Currently at least one day of data from 36 of these stations have been loaded into the Digital Ionogram Database (DIDBase). We also load into DIDBase all online Jicamarca (Peru) digisonde data (ionograms and auto-scaling results). More than 3 months of Roquetes (Spain) digisonde data (ionograms, auto-scaling, and manual scaling) has been loaded in permanent loading mode. Table 3 shows the current list of available station ionogram data that can be stored in DIDBase. Many years of retro data has been loaded into DIDBase for Grahamstown and Louisvale station (South Africa) and some more retro data for Sondrestrom.

Table 3. List of Worldwide Active Digisonde Stations Contributing to the DIDBase.

##	URSI	NAME	##	URSI	NAME
1.	AN438	ANYANG	21.	LM42B	LEARMONTH
2.	AS00Q	ASCENSION ISLAND	22.	LV12P	LOUISVALE
3.	AT138	ATHENS	23.	MU12K	MADIMBO
4.	BV53Q	BUNDOORA	24.	MHJ45	MILLSTONE HILL
5.	CAJ2M	CACHOEIRA PAULISTA			
6.	RL052	CHILTON		SH437	OSAN
			27.	PSJ5J	PORT STANLEY
8.	DB049	DOURBES	28.	PA836	*PT ARGUELLO
9.	DS932	DYESS AFB			
10.	EG931	EGLIN AFB		PRJ18	RAMEY
11.	EA036	EL ARENOSILLO	31.	PRJ18	ROME
12.	FF051	FAIRFORD	32.	EB040	ROQUETES
13.	FZA0M	FORTALEZA	33.	T139	SAN VITO
			34.	SA80K	SAO LUIS
16.	GR13L	GRAHAMSTOWN			
17.	HA419	HAINAN		TUJ20	TUCUMAN
18.	JI91J	JICAMARCA	38.	WP937	*WALLOPS
19.	JR055	JULIUSRUH	39.	WU430	WUHAN

Primary stations *Temporary down.

The DIDBase database holding ionograms, scaled, and edited data for the Cal/Val campaigns was moved to a new hardware platform based on Athlon MP 2200+ CPU, 140 GB SCSI RAID-5 disk array with a Linux operating system. The database is managed by the newly released open-source RDBMS "Firebird" version 1.0.2. The Firebird system allows unlimited connections from remote SAO-Explorer workstations via JDBC protocol over the Internet. Tests of DIDBase in its new configuration show reliable operations and improved speed. A new version of the SAO Explorer has been released, allowing queries to the "Characteristics" table of DIDBase. Retrieval of characteristics

for time series plots using this access mechanism is 2 to 10 times faster than the conventional reading of complete SAO records. The diagram for the DIDBase system is illustrated in Figure 21.

5.2 *ADRES Subsystem*

The ADRES subsystem was released and installed on an Application Server Computer. It consists of two Java-based programs DIDBFill (loading data into DIDBase) and DIDBReqPro (DIDBase Request Processor). The ADRES subsystem was tested to recreate reports for requests where data were manually rescaled. The new version software program SAOExplorer supports DIDBase to navigate and allow manual scaling of ionograms. "DIDB Calendar Inventory Tree" was added into SAOExplorer program to easily find what station list for any date interval is available.

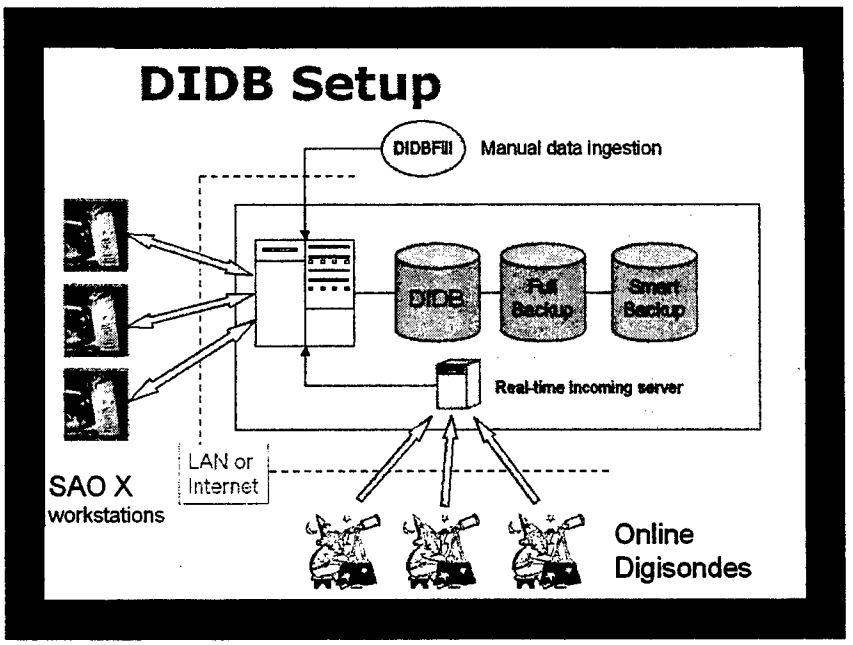

Figure 21. Illustration of the DIDBase Utilization Process

This DIDBase backup program is being developed to create a backup copy of the manually scaled data. The program has two types of backup: a full backup and a partial backup. Full backup saves all scaled data. The full backup is time-consuming and therefore it will run only once per month. The partial backup saves only the scaled data created or modified since the last partial or full backup and it runs every day. This approach saves these data every day reducing the risk of losing scaled data.

5.3 New Data "Dry Run" for TIMED/CEDAR Campaign

The campaign was conceptually aimed at coordinated radar/TIMED observations during a magnetic storm, however, if there were no storms during the campaign period, the radars would make some observations during non-storm times. The TIMED spacecraft carries the GUVI instrument, which is almost identical to the SSUSI instrument on DMSP. UMLCAR had an opportunity to do a dry run of the SSUSI

calibration/validation process, including coordination of observations with ionosondes. More than that, the ionosonde data could be used to verify global model predictions that arise from the radar data. Figure 22 describes the data collection and storage processes for a particular campaign in support of CAL/VAL.

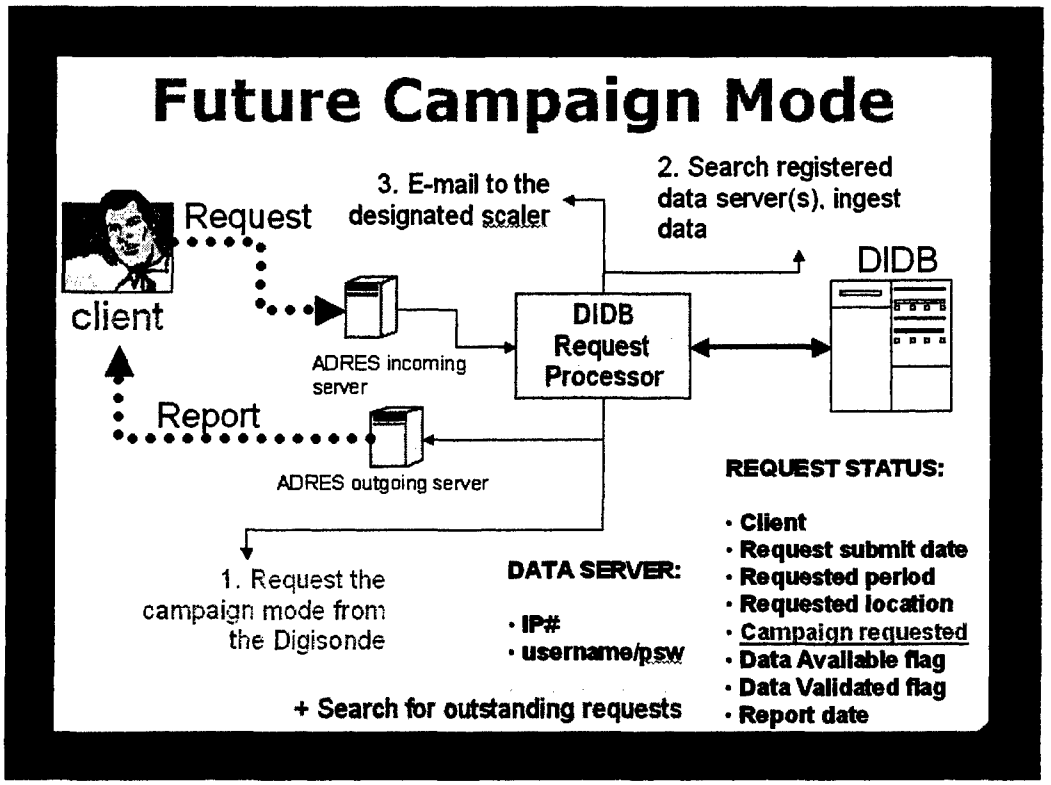

Figure 22. Flow Diagram for the Three-day Campaign for 11 Mid- and Low-Latitude Stations in the Western Hemisphere - 2002 April 25 – 27.

The following is the list of stations that contributed to this particular campaign.

#	URSI CODE	STATION NAME
1	WP937	Wallops Island
2	DS932	Dyess
3	AS00Q	Ascension Island
4	MHJ45	Millstone Hill
5	JI91J	Jicamarca
6	PSJ5J	Port Stanley
7	SAA0K	SAO LUIS
8	CAJ2M	CACHOEIRA PAULISTA
9	FZA0M	Fortaleza
10	EG931	Eglin
11	PA836	Pt Arguello

Thirty-five passes of the TIMED spacecraft over the stations were predicted and time intervals for requests were calculated. An example of this request list is shown below.

```
ADD
WP937, 2002.04.25 21:09:00, 2002.04.25 22:09:00
DS932, 2002.04.25 00:05:00, 2002.04.25 01:05:00
AS00Q, 2002.04.25 17:43:00, 2002.04.25 18:43:00
MHJ45, 2002.04.25 21:11:00, 2002.04.25 22:11:00
JI91J, 2002.04.25 20:56:00, 2002.04.25 21:56:00
PSJ5J, 2002.04.25 17:28:00, 2002.04.25 18:28:00
PSJ5J, 2002.04.25 19:08:00, 2002.04.25 20:08:00
SAA0K, 2002.04.25 19:21:00, 2002.04.25 20:21:00
CAJ2M, 2002.04.25 19:16:00, 2002.04.25 20:16:00
FZA0M, 2002.04.25 19:21:00, 2002.04.25 20:21:00
```

The digisonde software (both DPS-4 and DGS-256) was modified to support campaigns schedules. At the Millstone Hill digisonde a special observation (5 min time interval) mode was requested and ADRES subsystem automatically reprogrammed the sounding schedules. All data were collected and manually scaled.

The following list is an example of such a report.

```
[MHz]    [km] [TECU] [MHz]
2002.04.26 (116) 21:30:00  V    9.750  308.0   32.5   ---
2002.04.26 (116) 21:35:00  V    9.750  307.6   32.2   ---
2002.04.26 (116) 21:40:00  V    9.750  307.6   31.6   ---
2002.04.26 (116) 21:45:00  V    9.750  307.8   31.2   ---
2002.04.26 (116) 21:50:01  V    9.850  314.3   33.3   ---
2002.04.26 (116) 21:55:00  V    9.850  311.5   32.2   ---
2002.04.26 (116) 22:00:00  V    9.850  309.9   31.2   ---
2002.04.26 (116) 22:05:00  V    9.950  312.7   32.6   ---
2002.04.26 (116) 22:10:00  V    9.950  313.2   32.7   ---
2002.04.26 (116) 22:15:00  V    9.850  307.9   30.0   ---
2002.04.26 (116) 22:20:00  V    9.950  312.7   31.9   ---
2002.04.26 (116) 22:25:00  V    9.950  309.0   30.0   ---
```

5.4 Retrospective data "dry runs"

Two more dry run campaigns were performed for the CAL/VAL program. The first was a four-day campaign for 11 mid- and low-latitude stations in the Western Hemisphere (15–18April 2002). More than 4000 ionograms were collected and manually scaled. The second was on 31 May – 4 June 2002 for the same station list. Direct data exchange (request-report) using FTP at UMLCAR was used for both dry runs. Table 4 lists the stations and the dates that contributed to this test program.

Table 4. List of Stations Contributing to the Dry Run Test of the UMLCAR Data System for CAL/VAL

Station	April	May	June
CHILTON	21-26	31	1-4
ROQUETES	22-26	31	1-4
OKINAWA	22-26	31	1-4
EL ARENOSILLO	22-24	31	1-4
JULIUSRUH	22-26	31	1-4
ATHENS	22-26	31	1-4
GRAHAMSTOWN	22-26	31	1-4
BUNDOORA	22-26	31	1-4
LOUISVALE	22-26	31	1-4
HAINAN	21-26	31	1, 3, 4

5.5 Auroral E Scaling

Using data from the period 24-27 October 2000, a comparison was made of auroral E-layer profiles measured at Sondrestrom, Greenland using both the collocated digisonde and incoherent scatter radar. These data were collected every 5 minutes to provide high temporal resolution. On 17 Feb. 2001 more data was collected using 10 minute sampling. The results of these efforts were presented at the Cal/Val Working Group Meeting at the Applied Physics Laboratory. The title of the presentation was "Auroral E-Layer Profiles at Sondrestrom as seen by Digisonde and Incoherent Scatter Radar".

The results of this analysis show that both systems are able to provide a time history of auroral E density variations. The measurements show large spatial and temporal variations that might be expected of auroral E phenomena. The digisonde showed the simultaneous existence of several horizontally separated auroral E ionization structures within the sounder's field of view (~350 km diameter). Direct observation by a satellite should confirm the existence of these moderate scale structures. At times when only a single auroral E-layer is present, it is likely associated with diffuse aurora. SAOExplorer has been modified and tested to access DIDBase and the SPIDR database at NGDC. New features were added to facilitate access to the DIDBase inventory information. The new SAO format 4.3 was developed, which supports auroral E-layer

density profiles. The new format was added into NHPC and SAOExplorer, and the integrated program was tested.

This page left blank intentionally

References

Reinisch et al., 2000, The Radio Plasma Imager investigation on the IMAGE spacecraft, *Space Sci. Reviews*, **91**, 319-359.

Reinisch et al., 2003, Multistation digisonde observations of equatorial spread F in South America, submitted, *Annales Geophys.*

Oliver, B. M., R. M. Clements, and P. R. Smy, 1973, Experimental investigation of the low-frequency capacitive response of a plasma sheath, *J. Appl. Phys.*, **44**, 4511.